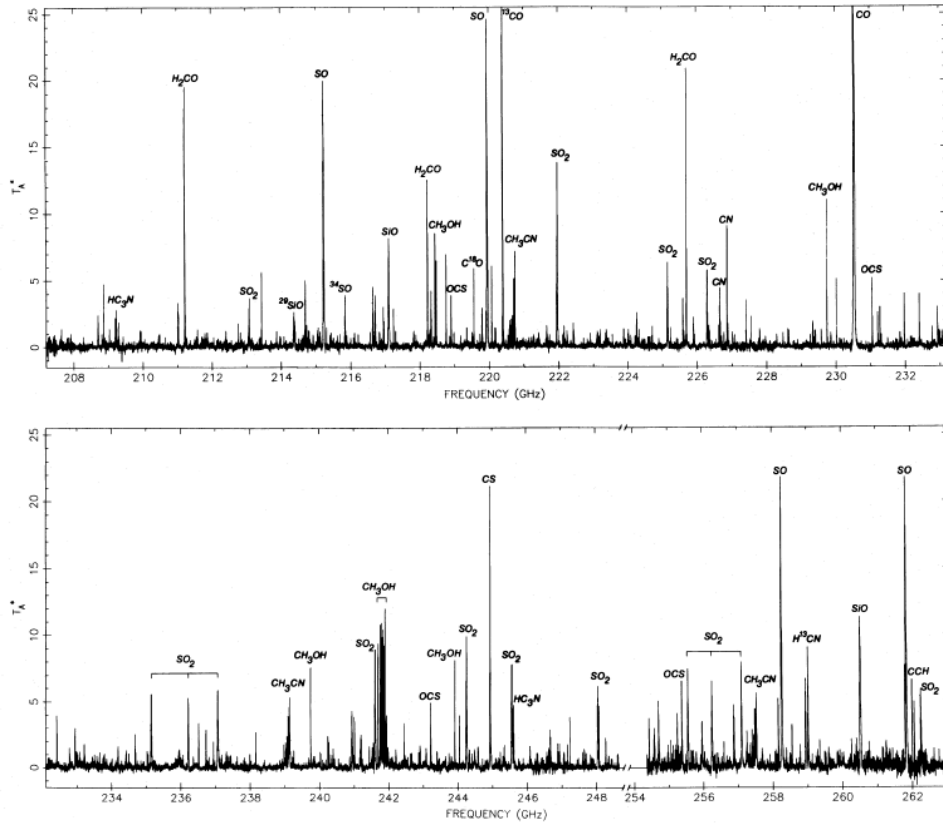# V Interstellar Molecules

Interstellar molecular gas was discovered in the 1940s with the observation of absorption bands from electronic transitions in CH, CH^+, and CN superimposed on the spectra of bright stars. In the late 1960s, centimeter- and millimeter-wavelength radio observations detected emission from rotational transitions of OH (hydroxyl), CO (carbon monoxide), NH_3 (ammonia), and H_2CO (formaldehyde). The Copernicus satellite detected Far-UV absorption bands of H_2 (the Lyman & Werner electronic transition bands) and HD in the early 1970s, and Lyman FUSE (launched in 1999) has detected diffuse H_2 along nearly every line of sight it has looked (where it often gets in the way of lines from the extragalactic sources of interest to the observations!). Infrared observations beginning in the 1970s detected H_2 in emission from forbidden rotational-vibrational transitions in the Near-IR, with advances in IR array detectors in the late 1990s greatly expanding studies of these transitions.

It was in the 1980s, with the development of new millimeter receiver technology, that the study of interstellar molecules blossomed. Many molecular species were identified, and the field has grown sufficiently in depth that we can only give it the most basic treatment here. This section will focus on the basic physics of molecular line formation in the interstellar medium, and on the properties of giant molecular clouds. These notes assume a familiarity with basic molecular structure (electronic, vibrational, and rotational quantum states) as was covered in the Astronomy 823 course (Theoretical Spectroscopy). Persons using these notes outside of OSU can refer to standard texts (like Herzberg) for the necessary background information.
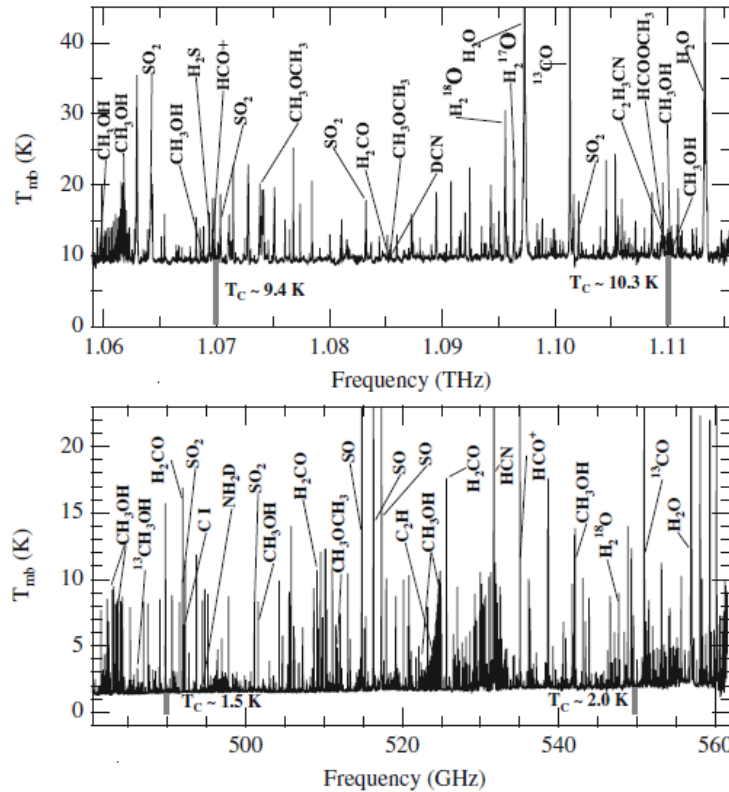
While the dominant molecular species in the ISM is H_2, because it is a homonuclear linear molecule with no permanent dipole moment all of the low-lying energy levels are quadrupole transitions with small transition probabilities (A-values) and relatively high excitation energies. The high excitation energies mean that these transitions are only excited at high temperatures or in strong UV radiation fields (i.e., fluorescence). Thus the most abundant molecule in the ISM, carrying most of the mass and playing a key role in excitation, thermal balance, and gas-phase chemistry, is virtually invisible to direct observation.

As a consequence, most of what we know about interstellar molecules comes from observations of so-called "tracer" species, primarily CO which is observed in its J=1−0 rotational transition at λ=2.6 mm. This and other molecular species are observed as emission lines from pure rotational transitions at centimeter to millimeter wavelengths. Like we saw in the case with the HI 21-cm line, we must account for stimulated emission as well as collisional and radiative effects when deriving the line properties. Since the formation of molecular species like CO occurs under conditions favorable for H_2 formation, we will try to estimate the amount of H_2 from the observed amount of CO with the assistance of a few simplifying assumptions.

A final aspect of the physics of molecular clouds is chemistry, both gas-phase and on the surfaces of dust grains. This is a rich topic that is sadly beyond the scope of this course.

Spectrum of Orion Molecular Cloud 1 (OMC1) in the 1.3mm band [Blake et al. 1987, ApJ, 315, 621] showing many of the 29 molecular species detected in this region.

Herschel HIFI spectra of Orion KL [Bergin et al. 2010, A&A, 521, L20]

V-1 Interstellar CO & Other "Tracer" Molecules

Radiative Transfer (yet again!)

In our discussion of the H$\scriptstyle\rm I$ 21cm line our treatment of radiative transfer included the effects of stimulated emission. We were assisted in this analysis by the fact that the 21cm wavelength of the transition is in the long wavelength Rayleigh-Jeans limit of the background radiation field. For the rotational transitions of interstellar molecules like CO[1] that occur at shorter wavelengths, this simplifying assumption is no longer true the analysis become more involved.

In general, the background radiation field has a blackbody spectrum:

$$I_\nu = B_\nu(T_R) = \frac{2h\nu^3}{c^2}\left[\frac{1}{e^{h\nu/kT_R}-1}\right]$$

where T_R is the brightness temperature of the background radiation field, which at millimeter wavelengths (e.g., for the CO J=1−0 transition at 2.6mm) is dominated by the cosmic microwave background radiation with $T_R \approx 2.725$K. We know from COBE and WMAP observations that the cosmic microwave background is the most perfect blackbody yet observed.

At millimeter wavelengths, the observed brightness temperature of a line $T_{b\nu}$ is often expressed in terms of an **effective antenna temperature**:

$$T_A^* = T_A/\eta$$

where η is the **receiver efficiency**. A molecular line source is usually observed by chopping the telescope's beam between on- and off-source positions and measuring the difference in antenna temperatures. In general, the difference in brightness temperatures is

$$\Delta T_A^* = (1-e^{-\tau})\frac{h\nu}{k}\left[\frac{1}{e^{h\nu/kT_{exc}}-1}-\frac{1}{e^{h\nu/kT_R}-1}\right]$$

The excitation temperature T_{exc} for a given transition is defined as:

$$\frac{n_u}{n_l} = \frac{g_u}{g_l}e^{-h\nu_{ul}/kT_{exc}}$$

For pure rotational transitions the excitation temperature is often called the **rotation temperature**, whereas for vibrational transitions it is called the **vibration temperature**. This nomenclature is analogous to the "spin temperature" defined for the H$\scriptstyle\rm I$ 21cm hyperfine transition.

The absorption optical depth is:

$$\tau_\nu = \int \kappa_\nu ds = \int (n_l B_{lu} - n_u B_{ul})I_\nu ds$$

On the right-hand side the first expression of the integrand is the pure absorption term, and the second is the stimulated emission term. Integrating the optical depth over the line profile and eliminating the B's as we did previously in our treatment of atomic gas line transfer gives

$$\int_{line}\tau_\nu d\nu = \frac{h\nu_{ul}}{c}\left(N_l B_{lu} - N_u B_{ul}\right) = \frac{c^2}{8\pi\nu_{ul}^2}A_{ul}N_u\left(e^{h\nu/kT_{exc}}-1\right)$$

---

[1] I will follow the usual convention of denoting the principal isotopic species of atoms in a molecule without giving the atomic weights explicitly. For example, "CO" means "^{12}C^{16}O". The isotopic species will be named explicitly when comparing different isotopic forms (e.g., when discussing the ^{12}CO/^{13}CO ratio in the "standard CO analysis").

where N_u is the column density of the molecules in the given upper excited state, and A_{ul} is the transition probability for the line. There are three regimes of excitation temperature:

$$T_{exc} = T_R : \ \Delta T_A^* = 0; \ \text{no line is visible}$$

$$T_{exc} > T_R : \ \Delta T_A^* > 0; \ \text{line appears in } \textit{emission}$$

$$T_{exc} < T_R : \ \Delta T_A^* < 0; \ \text{line appears in } \textit{absorption}$$

The excitation temperature will depend on the relative importance of radiative processes (which drive T_{exc} towards T_R) and collisional processes (which drive T_{exc} towards the kinetic temperature of the gas). Collisions between the molecular species in question (CO etc.) and HI and/or H_2 are the most important. Considering only a single collider for simplicity, the excitation temperature is:

$$\frac{1}{T_{exc}} = \frac{\left[\dfrac{1}{T_{kin}} + \left(\dfrac{A_{ul}}{nq_{ul}} \dfrac{T_R}{T_*} \right) \dfrac{1}{T_R} \right]}{\left[1 + \dfrac{A_{ul}}{nq_{ul}} \dfrac{T_R}{T_*} \right]}$$

where:

$$T_* = h\nu_{ul} / k \ \text{and}$$

$$nq_{ul} = \text{collisional de-excitation rate}$$

Written this way, the excitation temperature is a harmonic mean between the radiation and kinetic temperatures weighted by the relative collisional and radiative de-excitation terms. The ratio of the radiative and collisional rates is just the ratio of the density to the critical density for the transition:

$$n_{crit} = \frac{A_{ul}}{q_{ul}}$$

as we have seen previously for UV, optical, and near-infrared forbidden lines. In the low-density limit ($n < n_{crit}$), the excitation temperature is driven towards the radiation temperature and no line will be visible. In the high-density limit ($n \gg n_{crit}$), the excitation temperature is driven towards the kinetic temperature, and we see an emission line since $T_{kin} > T_R$ for most cases.
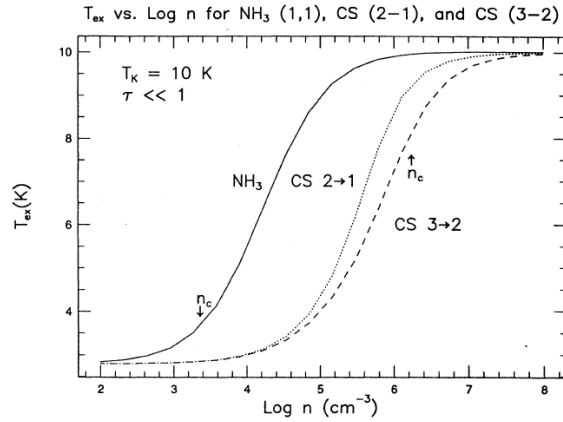
Critical Density and Line "Visibility"

At low densities, below the critical density, the excitation temperature will be only slightly above the radiation temperature and the emission line will be practically invisible. This is why you often read in the molecular line literature that a particular line is only "visible" at or above its critical density. At high densities, well above the critical density, the excitation temperature is at (or very near) the kinetic temperature of the gas, we often say that the line is "thermalized". Because different molecular lines have different critical densities, line visibility can serve as an approximate density diagnostic.

This rule of thumb is not without qualifications. Previously we noted that the weighting factor in the harmonic mean was the ratio of the density to the critical density. However, note that in the equation for $1/T_{exc}$, this factor is multiplied by an additional factor of (T_R/T_*). If stimulated emission is important, $T_* \ll T_R$, and the density must be much larger than n_{crit} to produce visible emission lines.

For example, the graph below shows the excitation temperature as a function of density for two molecular lines: the CS J=3–2 147 GHz line and the NH_3 (J,K)=(1,1) 23 GHz line. This CS line has a critical density of 1.5×10^6 cm^{-3}, and reaches an excitation temperature of $0.9T_{kin}$ at n=2×10^6 cm^{-3}. However, the NH_3 line has a critical density of 2×10^3 cm^{-3}, but the excitation temperature does not

approach the kinetic temperature until $n > 10^5$ cm^{-3}, nearly 3 orders of magnitude larger. The reason is the greater importance of stimulated emission at low frequencies compared to at high frequencies. In general, if $T_* = h\nu/k << T_{kin}$, the density must be much larger than the critical density in order for the line to be visible. As such, the density must be very large compared to the critical density to thermalize lines at centimeter wavelengths (like the NH_3 transition noted above), while at millimeter and sub-millimeter wavelengths, the lines of species like CO and CS are essentially thermalized at or near their critical densities. By the time you get to Infrared and Visible wavelengths stimulated emission becomes negligible and all collisionally excited lines thermalize at n_{crit}.

T_{exc} vs. density for NH_3 and CS transitions from Evans (1989)

Total Column Densities

Once the total optical depth and kinetic temperature have been measured, this only gives an estimate the column density for molecules in that particular rotational state. To convert this into a total column density, we can exploit the fact that in order for the line is visible at all it must be nearly thermalized. In the LTE approximation (limit where the level populations are "thermalized"), the fractional population of a given rotational state, J, is given as:

$$f_J = \frac{g_J e^{-E_J/kT}}{Q(T)}$$

where Q(T) is the partition function, defined as the sum over rotational states.

$$Q(T) = \sum_i g_i e^{-E_i/kT}$$

For rotational states in simple linear molecules like CO or CS, the statistical weights and energies of the Jth rotational state is:

$$g_J = (2J + 1)$$
$$E_J = J(J+1)hB(v)$$

Here B(v) is a function of the moment of inertia associated with vibrational quantum number v of the molecule (rotational transitions come in "ladders" within a given vibrational state)

$$B(v) = \frac{h}{8\pi^2 I(v)}$$

where $I(v)$ is the moment of inertia of the molecule when it is in vibrational quantum state v.

The summation is relatively straightforward to perform as it can be truncated at a high J level because transition probabilities increase with increasing J, and transitions out of these higher states occur fast enough that they will be heavily depopulated and contribute negligibly to the partition function.

At low density, the sum for Q(T) can be approximated as an integral:

$$Q(T) \approx \int (2J+1)e^{-E_J/kT}\,dJ$$

As the system becomes thermalized the partition function is approximately

$$Q(T) \rightarrow \frac{kT}{hB(\mathrm{v})}$$

For example, for the CO J=1−0 transition, the LTE partition function is:

$$Q(T) \approx \frac{T}{2.76\ \mathrm{K}}$$

Strictly speaking, thermalization (aka "LTE") is not always a valid assumption, and explicit non-LTE calculations are performed to solve the equations of statistical equilibrium to evaluate the partition functions. When you see a conversion between the observed CO J=1−0 flux to a total CO column density being computed in the "LTE approximation", you will know that they've followed the simple treatment described above.

Radiative Trapping

The preceding analysis has assumed that only photons from the background radiation field ("T_R") are used to compute the stimulated emission term, ignoring contributions from line photons. This assumption is only strictly true in an optically thin cloud. For strong lines in abundant molecular species, like the CO J=1−0 line, the cloud will be optically thick in these lines, and we will have to include stimulated emission from these emission-line photons in the radiative transfer treatment.

In an optically thick molecular cloud, line photons scatter around and are effectively "trapped". If the cloud is thick enough, the local density of line photons can greatly exceed the density of photons from the cosmic microwave background. These extra photons result in greater stimulated emission, driving the excitation temperature *above* the kinetic temperature of the gas. Further, the velocity field becomes important as we often observe that the widths of emission lines are larger than the expected thermal Doppler widths, either due to turbulent motions within the clouds or large-scale motions (e.g., velocity gradients or outflows).

There are a number of ways to calculate the effects of radiative trapping, the most common is the "escape probability" treatment of Scoville & Solomon [1974, ApJ, 187, L67]. The details are beyond the scope of these notes, but the basic idea is that radiative trapping causes line photons to scatter many times about the cloud, enhancing the subsequent emergent line flux due to stimulated emission. Each emission-line photon emitted by normal downward radiative transitions can effectively multiply itself by stimulated emission before escaping the cloud. The result is that you can get a *larger* excitation temperature at a *lower* density than in an optically thin cloud, thus lowering the effective density at which the line appears to "thermalize" and become visible.

Since CO J=1−0 line is always extremely optically thick in molecular clouds, some kind of radiative trapping treatment must be performed. For most Giant Molecular Clouds, the observed optical depths in the J=1−0 line are >10, lowering the effective density at which $T_{exc} \approx T_{kin}$ from 3000 cm^{-3} to as low as 300 cm^{-3}.

Density & Temperature Diagnostics

Density Diagnostics

There are a variety of ways to estimate the density of a molecular cloud from observations of molecular lines, all of which come with various assumptions and caveats. Goldsmith gives a

relatively complete list of the most common diagnostics in his review in *Interstellar Processes* along with citations to the key papers.

The most basic way to estimate density is from the observed column density by assuming a path length through the cloud:

$$\langle n \rangle \approx N_{tot} L^{-1}$$

N_{tot} is the total column density along the line of sight, and L is the path length.

A second way that is commonly encountered in the literature is to set lower limits on the density by noting which molecular lines of different critical densities are visible in a cloud. Some of the common emission lines (among many others) that are used in this way are:

Transition	Frequency	n_{crit}(10K)
^{12}CO J=1–0	115 GHz	~1000 cm^{-3}
NH$_3$ (1,1)	23.7 GHz	1800 cm^{-3}
CS J=1–0	49 GHz	4.6×10^4 cm^{-3}
HCO$^+$ J=1–0	4.3 GHz	1.7×10^5 cm^{-3}

If many lines from a given molecular species (e.g., H$_2$CO) can be observed, a better method is to measure the ratios of lines that are not yet thermalized ($n < n_{crit}$). These line ratios will be density sensitive and may be used to estimate densities in roughly the same way that we used the [SII] and [OII] doublet ratios at visible wavelengths in HII regions. Such ratios tend to have limited ranges of applicability, for example:

Lines	Applicable Range
CO J=1–0 and J=2–3	$10^{2.5} < n(H_2) < 10^4$ cm^{-3}
CS J=7–6 and J=4–3	$10^{5.5} < n(H_2) < 10^{7.5}$ cm^{-3}

The main limitation of using molecular line ratios as a density diagnostic is that detailed quantum mechanical calculations are required to work out the density dependence, and this has been done for only a few species with the sufficient precision.

A final way of estimating densities that is sometimes used to assume that the cloud is in virial equilibrium, with "turbulent" motions holding the cloud up against self gravity. Interpreting the observed line width as the virial velocity, you estimate the virial mass and divide by the volume of the cloud to estimate a density. Crude, but it can give a robust mean density for the cloud.

Temperature Diagnostics

The most important "thermometers" in molecular clouds are the rotational transitions of ^{12}CO. The low-J levels are very optically thick, and if the lines are thermalized, measuring the line strength gives the excitation temperature, and hence the kinetic temperature of the H$_2$.

In most molecular clouds without additional heating sources (i.e., away from regions of massive-star formation), the observed kinetic temperatures are in the range of 10–20K. In these regions, the thermal balance is between heating by cosmic rays and collisions with warm (T=30–40K) dust grains, and cooling by molecular line emission, with CO as one of the primary coolants. Near the edges of molecular clouds, heating by photoelectrons ejected by Interstellar Radiation Field photons becomes important. In clouds associated with massive-star formation (e.g., in Orion or M17), the cloud

temperatures range from 40–70K, and localized regions with heating sources can be as warm as a few 100K.

For a few molecular line species, we can estimate the kinetic temperature directly, along with an estimate of the density, using line ratios of optically thin transitions. Emission lines of NH_3, for example, are often used this way, in conjunction with detailed models. Again, the principal limitation of line ratio methods is the necessity of having using quantum mechanical models to predict the run of line ratios with density and temperature. Such data are known with sufficient precision for only a few molecular species.

Anomalous Excitation

Briefly, but not to diminish its importance, the complex quantum structure of molecules makes many of them susceptible to a variety of non-thermal excitation sources like radiative and collisional pumping. This can lead to anomalous under- or over-population of excited states if the combination of selection rules and transition probabilities works out just right.

If a molecule can be pumped so that the population of an excited state greatly exceeds the population of the ground state ("population inversion"), the excitation temperature can greatly exceed the background radiation temperature, and the additional population of the excited state enhances the effect of stimulated emission. Under the right circumstances, this can lead to the production of an astrophysical maser or laser (in laboratory spectroscopy, you get a "maser" if the wavelength is longer than 1mm, and a "laser" if shorter than 1mm). The most common astrophysical masers are OH, H_2O, and NH_3 masers powered by either radiative or collisional pumping. These masers are usually associated with regions of star formation, and in dusty outflows around AGB stars. This is an entirely separate field of endeavor beyond the scope of these notes, but the interested reader should consult Moshe Elitzur's review article in *Interstellar Processes*, or recent Annual Reviews articles on astrophysical masers.

If the anomalous excitation leads to significant *underpopulation* of an upper level relative to the lower level of a molecular transition, the resulting excitation temperature can become *lower* than the background temperature, causing the line to appear in *absorption* as against the cosmic background. An example of this is the "anomalous absorption" seen in formaldehyde (H_2CO), in which the upper level of the transition in question is depopulated by photon pumping into even higher levels. Collisional "refrigeration" mechanisms have also been proposed.

The Standard CO Analysis

As we saw before, the observed antenna temperature is (on-off) is:

$$\Delta T_A^* = \left(1 - e^{-\tau}\right) \frac{h\nu}{k} \left[f(T_{exc}) - f(T_R) \right]$$

where

$$f(T) = \frac{1}{e^{h\nu/kT} - 1}$$

Since the observed intensity depends on the excitation temperature, T_{exc}, and the optical depth, τ, observations of a single line will not allow you to derive both [i.e., you have two unknowns but only one observable].

Because the energy of a rotational transition E(J) is inversely proportional to the moment of inertia of the molecule I(v), changes in the isotopic species of one (or both) atoms will change the line frequency sufficiently to distinguish the two isotopic forms. For the CO molecule, the isotopic ratio is

^{13}C/^{12}C≈1/90, so that one expects the relative optical depth in the ^{13}CO lines to be smaller than in the ^{12}CO lines. This expectation is at the heart of the standard CO analysis: in most cases the ^{12}CO line is optically thick, while its isotopic partner ^{13}CO is optically thin. Observations show that the typical relative brightnesses of the J=1–0 line is I(^{13}CO)/I(^{12}CO)~0.05–0.4, in agreement with this expectation.

A further assumption is that ^{13}CO and ^{12}CO both arise in the same regions, and so share the same excitation temperature. If there are significant chemical fractionation effects, this assumption could be invalid (e.g., if local chemistry affects the creation/destruction of ^{13}CO differently than that of ^{12}CO).

In the limit of large optical depth for the ^{12}CO line, the excitation temperature is

$$T_{exc} = \frac{h\nu/k}{\ln\left(1+\dfrac{h\nu/k}{T_A^*(^{12}CO)+T_R}\right)}$$

Inserting the numbers for the J=1–0 line (hν/k=5.53K):

$$T_{exc} = \frac{5.53\ K}{\ln\left(1+\dfrac{5.53\ K}{T_A^*(^{12}CO)+T_R}\right)}$$

Here

$$T_A^* = \text{ observed effective line intensity of } ^{12}CO$$

$$T_R = \text{ background radiation field temperature (2.725K)}$$

For ^{13}CO, we assume that it is optically thin, and substitute in the T_{exc} derived from the ^{12}CO observations into the equation for the intensity of ^{13}CO and solve for the optical depth in ^{13}CO, τ(^{13}CO).

Because we expect that $T_{exc}>T_R$, the optical depth of the ^{13}CO line is

$$\tau(^{13}CO) \approx \ln\left[1-\frac{T_A^*(^{13}CO)}{T_A^*(^{12}CO)}\right]^{-1}$$

Otherwise, we would have to solve the equations using the full form for the effective antenna temperature, which would need to be done numerically.

The optical depth in ^{13}CO is then converted into a column density as follows:

$$N(^{13}CO) = 2.85\times10^{14}\,cm^{-2}\int\frac{\tau(^{13}CO)\left[1+T_{exc}\right]}{1-e^{-5.53/T_{exc}}}\,dv$$

The integral is taken over the line profile expressed as a function of line-of-sight velocity v. This column density is often written as $N^*(^{13}CO)$, as one assumes that if the line is visible it must therefore be thermalized, and so $T_{exc}≈T_{kin}$ and N^* is thus an "LTE" column density.

N(^{12}CO) is then derived by assuming an isotopic ratio for ^{13}CO/^{12}CO, usually the locally determined "cosmic" ratio of ~1/90.

V-2 Molecular Hydrogen (H_2)

Molecular Hydrogen (H_2) is the most abundant molecular species in the ISM, and plays a crucial role in cooling and molecular chemistry. Despite its importance, it is also the most difficult species to observe directly. The reason is that H_2 is a simple, homonuclear molecule. Because it consists of two atoms of identical mass, the center of mass and the center of charge coincide, resulting in no permanent dipole moment. With no dipole moment, only quadrupole rotational transitions can occur. This means that only the $\Delta J=0$ and $\Delta J=\pm 2$ rotational transitions occur, while the $\Delta J=\pm 1$ (dipole) rotational transitions are strictly forbidden. This means that unlike other molecules we have studied, H_2 emits no lines long-wavelength rotational lines.

The small mass and small size of the H_2 molecule gives it a low moment of inertia. This means that the first pure rotational transition, J=2–0, occurs at 28μm, a part of the spectrum unobservable from the ground due to water-vapor absorption in the atmosphere. Further, $h\nu/k$ =514K for this transition, very large relative to typical temperatures in giant molecular clouds (10–20K). The next pure rotational transition is J=4–2 at $\lambda\approx$12μm, which has $h\nu/k \approx$1200 K. The generally high energies of the first excited states of H_2 means that we expect negligible H_2 emission unless we are looking at unusually warm (500-1000K) H_2 gas in proximity to hot stars or in regions of active star formation within or at the fringes of giant molecular clouds. Contrast this situation with the CO J=1–0 line at λ=2.6mm where $h\nu/k$=5.53K and the molecule, which is easily excited by H_2 or HI collisions at temperatures of T=10–20K more typical of the cores of giant molecular clouds.

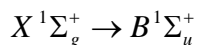In general, H_2 is only directly observable as

1. **Absorption** at Far-UV wavelengths in the diffuse ISM along sight lines toward nearby stars in the Lyman and Werner band electronic transitions. These lines arise in both cold and warm H_2. This is our only direct probe of the cold H_2 gas that makes up most of the ISM.

2. **Emission** by Infrared rotational-vibrational transitions in the electronic ground state of H_2 at wavelengths between 1 and 28μm in relatively warm regions. The molecular gas must be warm (500-2000K), excited either by shocks, outflows, or UV fluorescence from nearby stars.
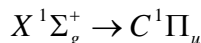
We will examine each of these below.

UV Lyman & Werner Bands

H_2 consists of 2 hydrogen atoms linked by a covalent bond (i.e., sharing electron pairs between the atoms). The lowest energy states of H_2 are shown in the figure below from Field, Somerville, & Dressler [1966, ARAA, 4, 207]. Subject to the usual selection rules for permitted electronic transitions ($\Delta\Lambda$=0,±1; ΔS=0) and symmetry constraints on H_2, there are two sets of allowed transitions out of the H_2 ground state:

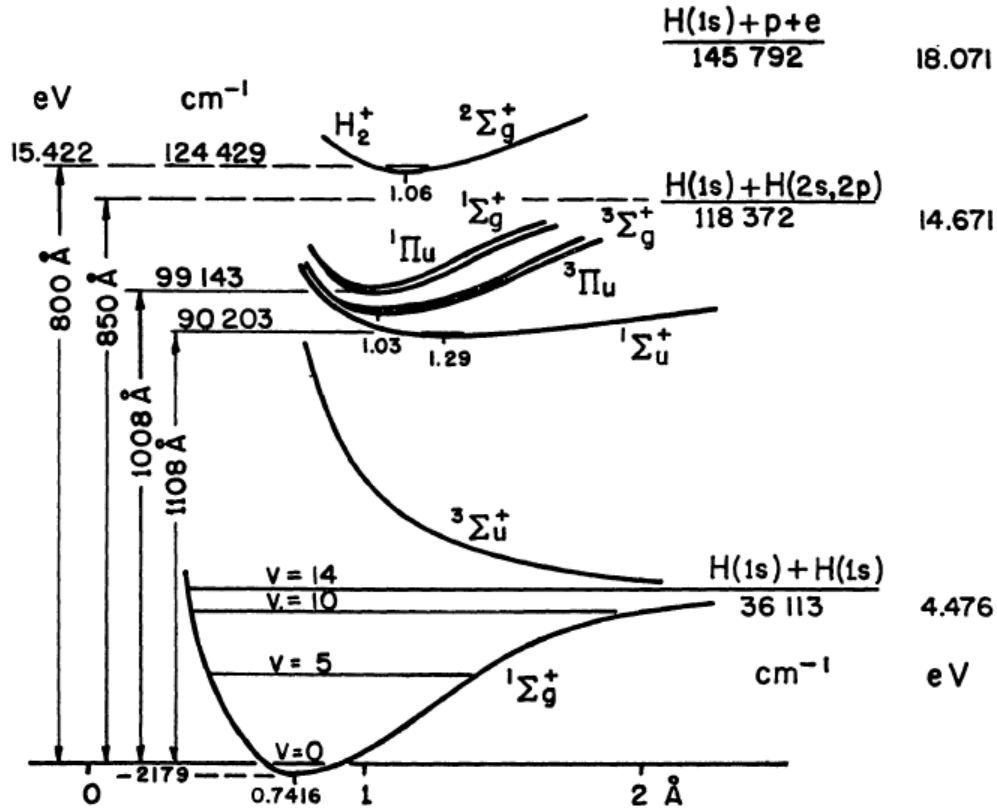> **Lyman Bands**: ΔE>11.2eV, λ<1108Å (first band head)

$$X\,^1\Sigma_g^+ \to B\,^1\Sigma_u^+$$

> **Werner Bands**: ΔE>12.3eV, λ<1008Å (first band head)

$$X\,^1\Sigma_g^+ \to C\,^1\Pi_u$$

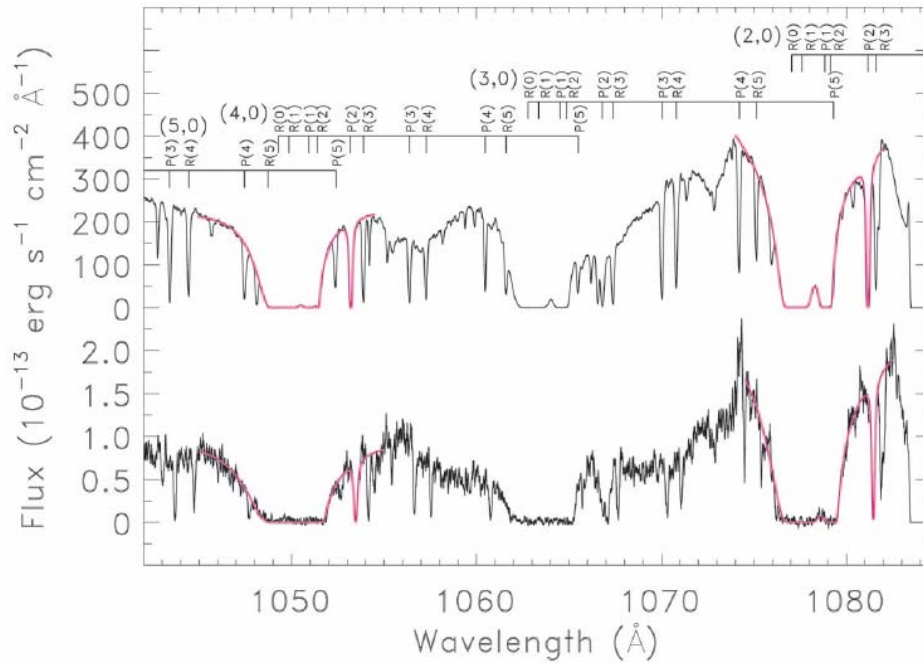Excitation into higher electronic states of H_2 requires photons with wavelengths shortward of 800Å. Since these photons are more likely to ionize HI (λ<912Å), these higher electronic transitions are generally suppressed. A complete list of transition probabilities and oscillator strengths for these

bands is given by Morton & Dinerstein 1976 [ApJ, 204, 1]. In all, the Lyman and Werner bands arising from the J=0–7 rotational levels in the ground vibrational state comprise nearly 400 absorption lines between 912 and 1120Å. An analogous set of HD (Deuterated Molecular Hydrogen) bands, shifted in wavelength, are also observed in this part of the spectrum. These, together with the HI and DI Lyman-series absorption lines, are potentially powerful diagnostics of atomic and molecular Hydrogen in the diffuse interstellar medium, a potential which until recently has gone unrealized.

Electronic states of H_2, from Field, Somerville & Dressler (1966)

The electronic absorption bands of H_2 occur in the Far-UV part of the spectrum inaccessible with either IUE or HST. Interstellar Lyman and Werner bands were first observed with the Copernicus satellite in 1974 (cf. Spitzer & Jenkins 1975, ARAA, 13, 133). Copernicus had very low sensitivity and could only detect these bands along relatively diffuse (e.g., A_V<1) lines of sight (e.g., towards ζ Puppis), although it did provide exceptional data. Later short-duration missions (IMAPS and ORFEUS) in the 1990s used small telescopes and their observations of the H_2 bands were limited to bright stars with relatively low line-of-sight extinction, and only a few targets due to their short mission times. Sounding rockets were used to study specific targets for very brief times. This all changed with the launch of the FUSE satellite in June 1999. FUSE is ~10^5 times more sensitive than Copernicus in the Far-UV band, and has produced must of the best data on the H_2 Lyman and Werner band absorption to date. This sensitivity has also allowed extension of these observations to so-called "translucent" line of sight, those with A_V>1 mag (e.g., Snow et al. 2000, ApJ, 538, L65, Rachford et al. 2001, ApJ, 555, 839 & 2002, ApJ, 577, 221). This particular study was one of the key projects for the FUSE mission.

FUSE spectra of the H_2 Lyman/Werner absorption bands along a translucent line of sight [From Rachford et al. 2002]

These absorption lines are the only way at present to directly detect the cold H_2 gas that makes up most of the ISM. The limitations of these bands as ISM diagnostics are the same as for the UV atomic absorption lines, namely that information is confined to particular lines of sight "back lit" by strong UV sources (e.g., OB stars or AGNs) with sufficiently low extinction that the UV light from the background source can be detected. However, because these absorption lines of H_2 are so strong, the H_2 Lyman/Werner bands have been seen along every line of sight where FUSE has observed, in fact they are often a foreground "nuisance" when observing extragalactic lines of sight, and in choosing targets one must take care not to pick sight lines where the strongest H_2 lines are expected to be saturated, as the redshifted lines of interest in, for example, an AGN have been known to fall into these bands.

The FUSE translucent cloud study produced direct measurements of the H_2 column densities from the J=0 and J=1 transitions along lines of sight to more than 40 early-type stars with A_V>1. Combined with earlier Copernicus data for diffuse lines of sight, the following general conclusions can be made:

1. The kinetic temperature of the H_2 gas range between ~50–100K, with a mean value around 70K. This temperature is uncorrelated with the amount extinction along a line of sight, but hotter H_2 gas can be found among diffuse lines of sight (i.e., there is greater scatter in T_{kin}, extending to higher temperatures), with cooler temperatures prevailing in regions where the H_2 column density becomes large enough for "self shielding" to become important.

2. The molecular fraction $f_{H_2} = 2N_{H_2}/(2N_{H_2} + N_{HI})$ is low ($<10^{-4}$) for sight lines with E(B−V)<0.08, then it increases abruptly to >0.01 because of the onset of self-shielding, and rises to as high as 0.8 with considerable scatter in translucent sight lines. Nowhere, however, does the molecular fraction get as large as 90% as expected by earlier theoretical models.

3. While there is no detailed correlation between the molecular fraction and color excess or R_V, the available data show that f_{H_2} is well correlated with the density-sensitive fractional CN abundance, the width of the 2175Å bump, and the slope of the far-UV extinction, and a
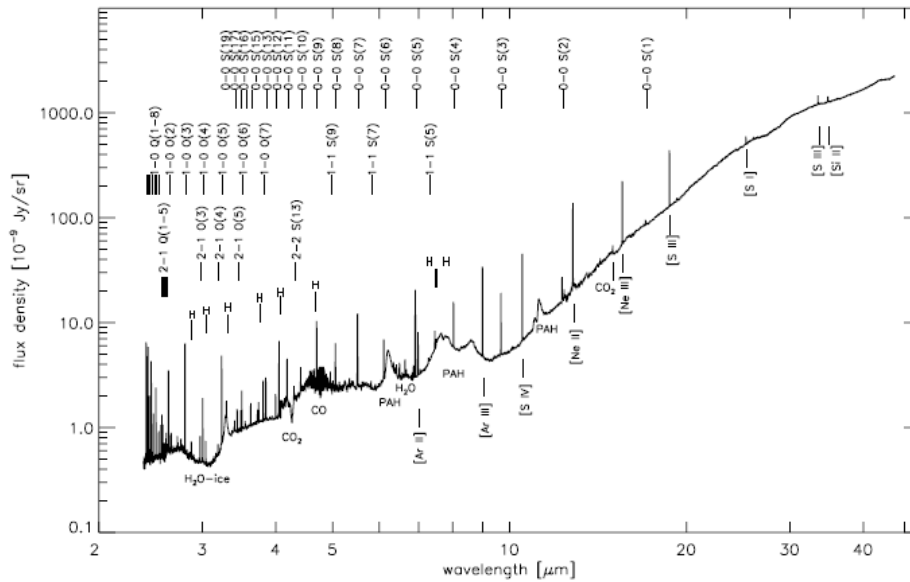
general trend for f_{H_2} to be anticorrelated with the kinetic temperature (hotter H_2 gas has a smaller molecular fraction). The relations with temperature and density are unsurprising: colder, denser clouds are expected to have a higher molecular fraction.

The H_2 electronic bands can, in principle, be seen in emission from the radiative cascade that would follow absorption of photons in the Lyman- and Werner bands. This would be most observable near regions with strong UV fluorescent excitation of H_2 (see below). In particular, there have been observations of emission-lines from high-lying Werner bands in the 1150-1950Å region accessible with IUE by Witt et al. 1989 [ApJ, 336, L21] towards a cold molecular cloud (the reflection nebula IC63), and by Schwartz et al. towards warm H_2 in Herbig-Haro objects (shocks associated with jet-like outflows from young stellar objects).

Near-Infrared Vibrational Rotational Emission Lines

Within the electronic ground state of H_2, all of the vibrational and rotational transitions are "forbidden" by the dipole selection rules. This means that the P- ($\Delta J=-1$) and R- ($\Delta J=+1$) branches of H_2 do not occur, but transitions in the O- ($\Delta J=-2$), Q- ($\Delta J=0$), and S- ($\Delta J=+2$) branches can occur and are observed in the near- and mid-infrared.

The first vibrational-rotational transition in the H_2 ground state is the $v=0$–$0S(0)$ transition, which is the $J=2$–0 transition at $\lambda=28.2\mu m$. All other vibrational-rotational transitions in the ground state have increasing energy (and shorter λ). Pure rotational lines ($v_u=v_l$) span the 3.4 to 28μm region, while $\Delta v=\pm 1$ vibrational-rotational transitions have typical energies of ~0.5eV and are found in the 1–4μm region clustering around 2μm. Typical transition probabilities are ~$10^{-7} - 10^{-8}$ sec^{-1}, so these lines are strongly forbidden.

ISO spectrum of Orion H_2 Peak 1 from 2-40μm showing a wealth of H_2 vibrational and rotational emission lines [Rosenthal et al. 2000, A&A, 356, 705]

The notation used for these lines is:

$$v_u - v_l \; O(J_l); \text{ for } \Delta J = -2$$
$$v_u - v_l \; Q(J_l); \text{ for } \Delta J = 0$$
$$v_u - v_l \; S(J_l); \text{ for } \Delta J = +2$$

For example, the 1–0S(1) emission line at λ=2.1218μm in the Near-IR arises from a transition between the (v,J)=(1,3) upper level and the (v,J)=(0,1) lower level in the electronic ground state of H_2.

H_2 has two spin isomers: **Para-Hydrogen** with the proton spins anti-parallel, corresponding to the even-numbered J states, and **Ortho-Hydrogen** with the proton spins parallel, corresponding to odd-numbered J states. The **ortho-to-para ratio** is 3.0 for thermalized level populations (75% ortho-H_2 and 25% para-H_2). Because only ΔJ=0,±2 radiative transitions can occur, radiative transitions between the various rotational-vibrational levels in the ground state will preserve the ortho- or para-state of the molecules, and so one speaks of separate ortho and para energy "ladders" within the ground electronic state. Deviations from the predicted ortho-to-para ratio of 3 are primarily caused radiative de-excitation from the excited Lyman- or Werner-bands into ortho or para ladders in the ground state, and thus observations of different ortho-to-para ratios is taken as a sign of fluorescent excitation by UV photons.

Because the rotational-vibrational states have typical transition energies of 0.5eV, they require excitation temperatures of ~1000 K. Since the kinetic temperature of typical cold molecular clouds is at most a few 10s of Kelvins, this means that you will only see these lines in regions that are unusually energetic. There are three basic mechanisms for exciting the NIR rotational-vibrational emission lines of H_2 in nebulae:

1. **Collisional Excitation:** This primarily affects the low-J levels of H_2. Hydrodynamic shocks with velocities of >6 km/sec are the principal cause of strong collisional excitation, but if the velocity is >25 km/sec, the shock will destroy (dissociate) H_2.

2. **UV Fluorescence:** Radiative excitation of the Lyman and Werner bands by UV photons is followed by radiative de-excitation into excited states of the ground level which "pumps" the populations of the excited states.

3. **Formation Excitation:** Excitation of low-lying states as a by-product of molecular formation on grains due to the redistribution of binding energy between heating of the grain surface, kinetic energy of the ejected molecule, and internal excitation of the newly-formed H_2.

We shall consider each of these in turn.

Collisional Excitation

H_2 molecules are subject to collisions in a variety of astrophysical environments, particularly in regions with hydrodynamic shocks such as jets from young stellar objects, stellar winds impinging upon interstellar clouds, or shocks in supernova remnants. Because the first (v=1) vibrational excited state of H_2 lies ~0.5eV above the ground state (corresponding to E/k≈6000K), temperatures above ~1000K are required to collisionally excite the low-lying vibrational levels of H_2. Because the dissociation rate of H_2 increases very rapidly with temperature, molecular gas hotter than 4000-5000K will either rapidly dissociate into HI or cool dramatically (H_2 dissociation is a very efficient cooling mechanism). As such, most collisional excitation of H_2 will occur for molecular gas in a very narrow range of a few thousand Kelvins.

Models of shocks show that the excitation of the low-J states responsible for the observed rotational-vibration levels occurs if the shock speed is faster than ~6 km/sec, with an excitation efficiency that scales roughly like $n_0 v^3$, where n_0 is the pre-shock density and v is the shock speed. At shock speeds >25 km/sec, the shock heating results in dissociated into atomic Hydrogen, but one may still get excitation due to re-formation behind the shock as the post-shock gas and dust grains cool off.

Because of the narrow range of excitation temperatures between the lower threshold and the upper dissociation/cooling threshold, collisionally excited H_2 is characterized by strong lines of low vibrational levels (v<4), with rapidly decreasing level populations with increasing energy levels.

In the high-density limit where collisional excitation and de-excitation will dominate, the relative H_2 vibrational-rotational level populations $n_{v,J}$ are characterized by a "thermalized" Boltzmann population:

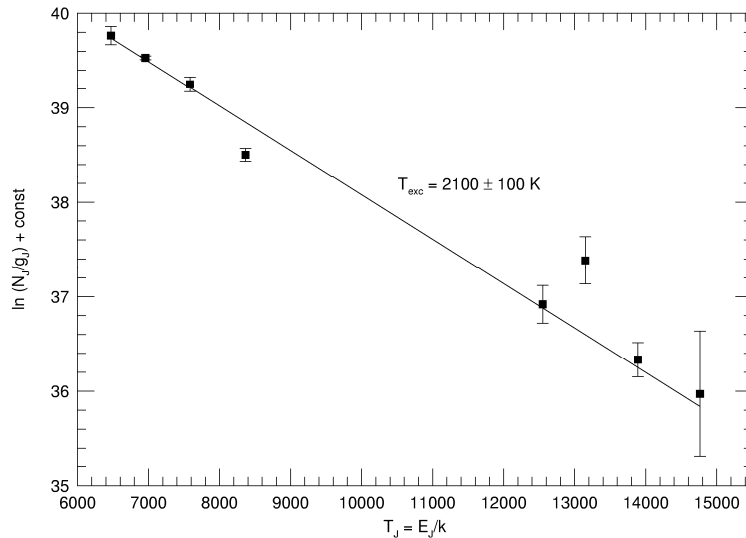$$\frac{n_{v,J}}{g_J} \propto \exp\left[-\frac{E_{v,J}}{kT}\right]$$

where g_J is the statistical weight of the level, $E_{v,J}$ is the energy of the upper level, and T is the kinetic temperature of the gas. For odd-numbered J-levels (ortho-H_2), the statistical weight is:

$$g_J = 3(2J+1)$$

while for the even-numbered J-levels (para-H_2), the statistical weight is
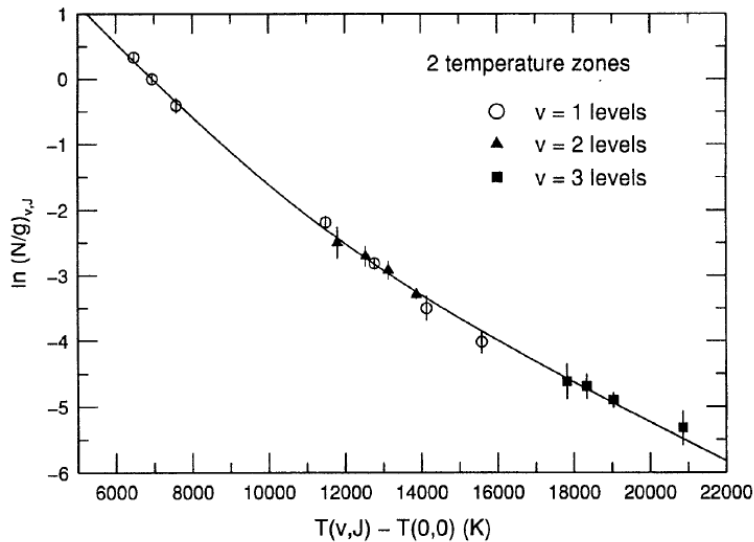
$$g_J = 2J+1$$

The standard analysis for the rotational-vibrational states of H_2 is to create an **Excitation Diagram** that plots the emission line data as $\ln(n_{v,J}/g_J)$ as a function of $(E_{v,J}/k)$. The line strengths are usually expressed relative to a strong H_2 line like the v=1−0S(1) λ2.1218μm line. If the level populations are thermalized, they will all lie along a straight-line locus in this diagram with a slope inversely proportional to the excitation temperature of the gas. An example excitation diagram for a collisionally excited region in the starburst galaxy NGC6240 is shown below.

Excitation diagram for near-IR H_2 lines in NGC6240 (unpublished OSIRIS data)

If a range of temperatures occurs along the line of sight (e.g., your sight line integrates through the cooling region behind a shock), the diagram will show a smoothly curving locus of points, with lower energy levels lying along a steeply sloped (lower T) curve, with more highly-excited levels lying along a flatter-sloped curve because these levels are only excited at higher temperatures. An example of this is shown below for the bright near-IR H_2 peak in the Orion Molecular Cloud (OMC "Peak 1") from Everett, DePoy & Pogge 1995 [AJ, 110, 1295]. The curves are fits assuming a power-law cooling function responsible for the range of temperatures observed. As advertised, the low-lying levels have a steeper slope (lower excitation temperature) than the high-lying levels (shallower slope, hence higher excitation temperature).

Excitation Diagram for near-IR H_2 emission lines in Orion H_2 Peak 1 [Everett et al. 1995]

At lower densities, radiative de-excitation from excited rotational-vibrational states becomes important for determining the relative H_2 level populations. Because each energy level has a different critical density, you need to specify both the density and temperature to estimate the equilibrium H_2 populations. Such level populations will not be thermalized per se, and the temperature derived from the slope of the data in the excitation diagram is more correctly an excitation temperature rather than a reasonable approximation of the kinetic temperature.

Which colliding species dominates (atoms or other molecules) determines the densities at which the observed relative level populations will deviate from the predicted high-density thermalized (near-LTE) populations. This is because each different collider has a different critical density associated with it. In purely molecular regions where H_2-H_2 collisions dominate, the critical densities are relatively high: 10^{5-6} cm^{-3}. In partially atomic gas, H^0-H_2 collisions begin to dominate when the atomic fraction is $H^0/H_2 > 0.01$ because the critical densities for H^0-H_2 collisions are about 2 order of magnitude lower than for H_2-H_2 collisions. In this case, the level populations will fall below the LTE predictions at densities of $\sim 10^3$ cm^{-3}. In either case, where a sufficient number of Near-IR H_2 lines have been observed to make these subtle deviations evident, detailed level calculations are required to fully understand them (see Martin, Schwarz & Mandy 1996 ApJ, 461, 256, and Everett 1997, ApJ, 478, 246).

Fluorescent Excitation

In the interstellar medium, H_2 in the electronic ground state can be excited into the first or second electronic excited states by absorption of a UV photon in the Lyman or Werner bands, respectively. Excitation is followed by radiative de-excitation back into the electronic ground state. On average, $\sim 12\%$ of the excited H_2 molecules will de-excite into the dissociation bands ($v>13$) of the ground state, destroying the molecule (see below). The remaining, however, de-excite into bound levels of the ground electronic state which at low densities will cascade downwards into the $v=0$ level by radiative de-excitation through the forbidden rotational-vibrational transitions described before. At very high densities ($>10^5$ cm^{-3}, the critical densities of the rotational-vibrational states), the populations of these excited states can be redistributed by collisions before de-excitation into the $v=0$ level. Similarly at high UV flux densities multiple fluorescent excitations can redistribute the excited ground-level populations.
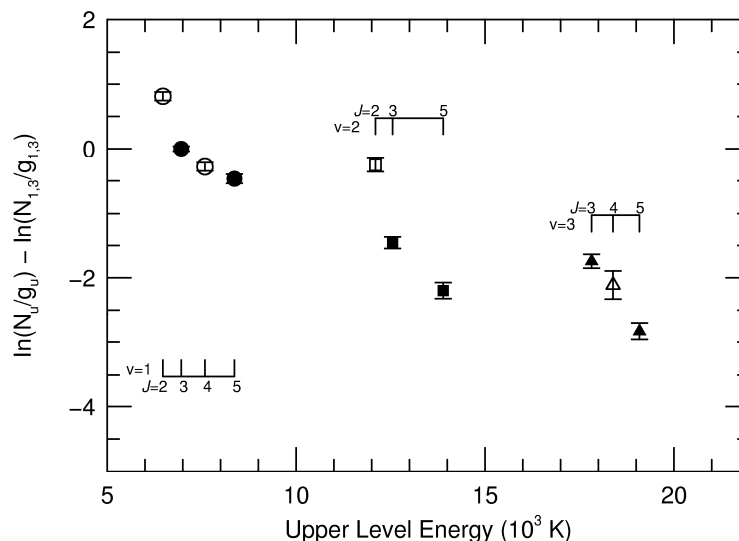
In addition to fluorescence by absorption of Far-UV continuum photons, the 1–2R(6) and 1–2P(5) transitions in the H_2 Lyman band are in near-resonance with the HI Lyman-α line at Doppler shifts of +15 and +100 km/sec respectively. Strong shocks can produce significant Lyman-α emission, which in turn can fluorescently pump H_2. This has been implicated as a possible source of warm H_2 emission at the working surfaces of jets emerging from Young Stellar Objects (e.g., Wolfire & Königl 1991 ApJ, 383, 205).

Because the rotational state of the molecule changes very little during excitation and de-excitation (only $\Delta J=0,\pm2$ transitions can occur), the rotational level populations will reflect the rotational state of the original gas being illuminated by UV radiation, whereas collisions can result in rotational mixing.

In general, the spectral signatures of low-density fluorescent excitation of H_2 are threefold:

1. Significant population of high-lying (v>4) vibrational levels that are rarely populated by collisions as they have sufficiently small Boltzmann factors that make these higher vibrational states relatively inaccessible.

2. Excitation temperatures for rotational states within a given vibrational level ("rotation temperatures") are lower than the excitation temperatures among vibrational levels at a given rotational state ("vibrational temperatures). In collisionally excited systems, rotational and vibrational temperatures are the same. The effect of this is to split the simple locus in the excitation diagram into separate curves by vibrational level.

3. The populations of even-numbered rotational states (para-H_2) are enhanced relative to odd-numbered states (ortho-H_2), in the sense that the observed ortho-to-para ratio will be smaller than the value of 3 expected for a thermalized population.

An example of an excitation diagram for fluorescently-excited H_2 gas in the reflection nebula NGC 7023 from Martini et al. 1997 [ApJ, 484, 296] is shown below.

Excitation diagram of fluorescent H_2 lines in NGC 7023 (adapted from Martini et al. 1997)

The effects of fluorescent excitation are most dramatic among the high vibrational levels (v=5, 6, and 7) that occur primarily in the 1–1.8μm region (J and H-bands) and are unlikely to be significantly populated by collisions. The spectral signature of fluorescently excited H_2 emission has been observed in reflection nebulae (Hayashi et al. 1985 MNRAS 215, 31P, Sellgren 1986 ApJ, 305, 399; Martini, Sellgren & Hora 1997, ApJ, 484, 296; Martini, Sellgren, & DePoy 1997, ApJ, 484, 296), and planetary nebulae (Dinerstein et al. 1988 ApJ 327, L27).

The signatures of fluorescent excitation, however, can be effectively erased at high densities when collisions start to become important. If the density is high enough ($>10^{4-5}$ cm^{-3}), collisions can thermalize the level populations, resulting in excitation diagrams that more closely resemble shock-heated H_2, even when UV fluorescence is important. The effect of collisions is to quickly de-populate the high vibrational levels whose lines are usually an unambiguous signature of fluorescent excitation. The converse, however, does not occur: there is no convincing combination of effects that will cause a collisionally excited region to emit like a fluorescently excitation region.

In any case, the detailed predictions of fluorescent excitation models depend sensitively on the density, temperature, UV radiation field intensity & spectrum, H_2 formation/reformation processes etc. Classic fluorescent models are those of Black & van Dishoeck (1987 ApJ, 322, 412) and Draine & Bertoldi (1996, ApJ, 468, 269). These are the ones that are most often compared with observations.
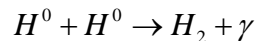
Formation Excitation

H_2 molecules form most efficiently on the surfaces of dust grains. Upon formation, the 4.5eV binding energy must be distributed into kinetic energy (after breaking the bond with the grain surface), heating of the dust grain at the formation site, and internal energy in the form of excitation of rotational-vibrational states within the electronic ground state. The exact distribution of energy depends on the details of formation that are fundamentally unknown, and so formation excitation is difficult to assess observationally. An example is higher-than-expected excitation temperatures in H_2 Lyman-Werner bands observed in absorption towards stars (e.g., Spitzer & Zweibel 1974, ApJ, 191, L127).

Some models have tried to include formation excitation in an ad-hoc way. For example the models of Black & van Dishoeck (1987) considered three different distribution functions in which (1) 1.5eV was distributed among the rotational-vibrational levels following the Boltzmann distribution, (2) all H_2 molecules from in the v=14, J=0,1 levels, and (3) all H_2 molecules form in the v=6 level with low-J states. These are then used as inputs in computing the emergent spectrum (see Black & van Dishoeck 1987 and Le Bourlot et al. 1995 ApJ, 449, 178 for examples).
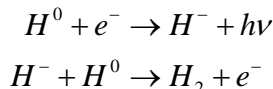
Formation of H_2

There are two primary ways that H_2 can be formed in the gas-phase. The first is **Direct Radiative Attachment** in which two H atoms collide to form H_2 followed by radiation of the excess 4.5eV binding energy as photons:

$$H^0 + H^0 \rightarrow H_2 + \gamma$$

After the H^0-H^0 collision the binding energy is converted into internal energy (excitation of rotational-vibrational levels of the ground state) in newly-formed H_2 molecule. Because these transitions are highly forbidden, with small Einstein A coefficients, radiation of the binding energy very inefficient, and the molecule is much more likely to dissociate before it relaxes. The rate coefficient for radiative attachment is $<10^{-23}$ cm^3 s^{-1}, so this mechanism is much too slow and inefficient to form H_2 in sufficient quantities to be important in the ISM. Three-body processes, in which three H^0 atoms collide and the third H^0 atom carries off the excess binding energy, are similarly unlikely at ISM densities, though they have been proposed as a way to form H_2 in protoplanetary disks.

The second gas-phase mechanism is **Associative Detachment**, which was first proposed by McDowell [1961, The Observatory, 81, 240] and given its classic treatment by Dalgarno & McCray [1973, ApJ, 181, 95].

$$H^0 + e^- \rightarrow H^- + h\nu$$
$$H^- + H^0 \rightarrow H_2 + e^-$$

The first reaction, **Radiative Association**, is slow, having a temperature-dependent rate coefficient of $\sim 10^{-18}\,T\,\mathrm{cm}^3\,\mathrm{s}^{-1}$. The second reaction, **Associative Detachment**, is much faster with a nearly temperature-independent rate coefficient of $\sim 1.3 \times 10^{-9}\,\mathrm{cm}^3\,\mathrm{s}^{-1}$, though this step will have to compete with photodissociation of H^- which has a rate of $\sim 2.4 \times 10^{-7}\,\mathrm{s}^{-1}$ for diffuse clouds exposed to the ISRF. The combined volumetric H_2 formation rate for this mechanism is approximately

$$\frac{dn_{H2}}{dt} \simeq 7.5 \times 10^{-23} \left(\frac{T}{100\mathrm{K}} \right) \left(\frac{x_e}{1.4 \times 10^{-4}} \right) n_H n_{H^0}\ \mathrm{cm}^{-3}\ \mathrm{s}^{-1}$$

Overall, this mechanism is also very inefficient at forming H_2 in the ISM, especially at low temperatures (though it is about an order of magnitude faster than direct radiative attachment). While too slow to explain the observed abundances of H_2 in the present-day ISM, it may be important in the early universe when no metals, and hence no dust grains, were present, but the gas was hotter (larger T) and there were copious electrons present from partial ionization of H^0 (larger x_e)

The currently favored H_2 formation mechanism is **Grain-Surface Catalysis**, first described by McCrae & McNally [1960, MNRAS, 121, 238] and given its classic treatment by Gould & Salpeter [1963, ApJ, 138, 393]. An H atom colliding with a dust grain will have a certain probability of sticking to the surface, provided that it is not moving too fast (e.g., as in a hot HI gas) and that the grains themselves are not too hot, which makes the surfaces energetically less "sticky". Once the H atom has been adsorbed by the grain surface, it will migrate around until it reaches a site on the grain surface where it is more tightly bound by either chemisorption (i.e., bound by valence forces with surface materials) or physisorption (i.e., bound by intermolecular van der Waals forces). Such sites act as "sinks" for H atoms. It is while trapped in this site that the atom is likely to encounter another H atom, and the two can react to form H_2, distributing the 4.5eV of binding energy into (1) heating of the dust grain, (2) breaking the "activation barrier" at the formation site and ejecting the newly-formed H_2 molecule from the surface ("desorption"), and (3) internal vibrational energy (excited ground states) that is later radiated away by the molecule as rotational-vibrational emission lines.

The volumetric rate of dust-catalyzed H_2 formation is given by:

$$\frac{dn_{H2}}{dt} = R_d n_H n_{H^0}$$

where n_H is the total density of hydrogen of all forms ($n_H = n_H^0 + 2n_{H2}$), n_H^0 is the density of neutral atomic hydrogen, and R is a rate coefficient with units of $\mathrm{cm}^3\,\mathrm{s}^{-1}$ that depends on the temperature of the atoms and grains and the fraction of atoms that can adhere to the grain:

$$R_d = \frac{1}{2} \left(\frac{8kT}{\pi m_H} \right)^{1/2} \int da\, \frac{1}{n_H} \frac{dn_{gr}}{da} \pi a^2 \gamma(a)$$

Here $\gamma(a)$ is the probability of sticking to a grain of size a. In general, it appears that all H atoms will stick to grains if their speeds are <2km/sec, provided that the grain temperatures are between ~ 20–100K. If the grains are too hot, the adsorbed atoms will evaporate off the grain surface before they can find another H atom and form H_2.

From observations of the fraction of H_2 towards nearby stars using Far-UV measurements of the Lyman-Werner bands, the H_2 formation rate coefficient is estimated to be $R_d \approx 1$–$3 \times 10^{-17}\,\mathrm{cm}^3\,\mathrm{s}^{-1}$, implying a mean sticking fraction of $\langle \gamma \rangle \approx 0.06$ for typical interstellar conditions and the observed dust/gas ratio. Draine & Bertoldi [1996, ApJ, 468, 269] quote $R_d = 6 \times 10^{-18} T^{1/2}\,\mathrm{cm}^3\,\mathrm{s}^{-1}$. Thus while very small grains have most the total grain surface area, they are expected to be less effective as H_2

formation sites, and most molecular formation thus occurs on larger grains. In some sense this is not surprising, as the smaller the grain becomes, the longer the timescale between H-atom collisions. The H-atom **impact timescale**

$$t_{HI} \approx 8 \times 10^4 \text{ s} \left(\frac{a}{0.01 \mu m} \right)^{-2} \left(\frac{n_H}{30 \text{ cm}^{-3}} \right)^{-1} \left(\frac{T}{100K} \right)^{-1/2}$$

For typical interstellar conditions, t_{HI} is of order the photon absorption time. As we saw in the previous section on Dust, the absorption of a single photon by a small grain can cause rapid stochastic heating of the grain. Thus in the time it takes 2 H atoms to collide with and stick to a small grain it is very likely that a photon will be absorbed with enough energy to kick off the one or both of the hydrogen atoms, effectively suppressing H_2 formation on tiny grains. Such photons have a less dramatic effect on the temperatures of large grains, and so photosuppression of H_2 formation will be less effective.

The corresponding timescale for H_2 formation on grains, t_{H2} is:

$$t_{H2} \approx 10^9 n_H^{-1} \text{ years}$$

For typical interstellar cold interstellar clouds where densities are of order 10^4 cm^{-3} it is possible to convert most of the HI into H_2 in as little as 10^5 years. Interstellar shocks may speed up this process by making the gas warmer and denser, provided the shocks are not so strong as to destroy the grains or the newly formed molecules.

Some other important papers on H_2 formation on grains are Hollenbach & Salpeter 1971 [ApJ, 163, 155] and Hollenbach & McKee 1979 [ApJS, 41, 555], and discussion in Draine & Bertoldi 1996 [ApJ, 468, 269].

Destruction of H₂ Molecules

H_2 molecules can be destroyed collisions and by UV photons (photodissociation). Collisional dissociation occurs at temperatures >4000 K, when collisions with HI can excite H_2 into the unbound $v>13$ vibrational states. Photodissociation of H_2 occurs when UV photons (either from a nearby star of the ISRF) are absorbed with sufficient energy to unbind the molecule.

There are two possible processes for photodissociation:

Direct Photodissociation from the electronic ground state:
An H_2 molecule in the $X^1\Sigma_g^+$ ground state should dissociate if it absorbs a photon with an energy >14.7eV (λ<850Å). The problem with this mechanism is that there are two processes competing for these photons. The first is HI ionization (threshold of 13.6eV, λ=912Å), which has a higher cross-section, so such photons are more likely to photoionize HI than dissociate H_2. Second, the threshold for photoionization of H_2 to H_2^+ out of the ground state is $h\nu$>15.5eV (λ<804Å), which also has a larger cross-section than photodissociation. Thus while direct photodissociation can occur, it is very inefficient.

UV Fluorescent Photodissociation
This is a two-step process in which absorption of Lyman- or Werner-band UV photons is followed by radiative de-excitation into ground state "vibrational continuum" bands which have vibration quantum numbers $v>13$. These high vibrational levels are unbound and the molecule dissociates, converting binding energy into the kinetic energy of the now free H^0 atoms. On average ~12% of all radiative decays following absorption in the Lyman- and Werner-bands

results in fluorescent dissociation of H_2. This is the dominant mechanism for H_2 photodissociation in the ISM.

Classic papers describing these H_2 destruction are Dalgarno & Roberge [1979, ApJ, 233, L25 for collisional dissociation] and Black & Dalgarno [1976, ApJ, 203, 132 for photodissociation].

The rate of photodissociation via Lyman/Werner band fluorescence is

$$\zeta_{diss} = \int 4\pi J_\nu \sigma_\nu k_\nu d\nu$$

where $4\pi J_\nu$ is the strength of the radiation field (e.g., the ISRF in the diffuse ISM), k_ν is the fraction of Lyman/Werner band excitations that are followed by de-excitation into the vibrational continuum band and lead to dissociation of H_2 ($k_\nu \approx 0.12$ for the ISRF), and σ_ν is the cross-section for Lyman-Werner fluorescence

$$\sigma_\nu = \sum_i \bar{\sigma}_i \phi_{\nu i}$$

where the sum is over all Lyman/Werner bands with $h\nu < 13.6 \text{eV}$ (i.e., absorptions arising from photons less energetic than the HI ionization potential).

The rate of H_2 destruction via this process is

$$\frac{dn_{H_2}}{dt} = -\zeta_{diss} n_{H_2}$$

In the diffuse ISM, equilibrium between grain formation and fluorescent photodissociation occurs when

$$R_d n_H n_{H^0} \approx \zeta_{diss} n_{H_2}$$

For typical values of the rate coefficients in the diffuse ISM, $\zeta_{diss} \approx 5.5 \times 10^{-11} \text{ s}^{-1}$, and so the fraction of H_2 relative to Hydrogen of all forms in the diffuse ISM is roughly

$$\frac{n_{H_2}}{n_H} \approx 1.1 \times 10^{-7} T^{1/2} n_H$$

In the diffuse ISM, the time to achieve equilibrium should be of order $1/\zeta_{diss}$, which is ~600 years for typical conditions. We thus expect that in the diffuse ISM, the fractional abundance of H_2 that we observe along virtually all sightlines is in equilibrium.

Self-Shielding

At H_2 column densities $>10^{14} \text{ cm}^{-2}$ the Lyman/Werner UV absorption line bands start to become optically thick, and H_2 becomes **self-shielding** in the sense that all of the photons that could lead to UV fluorescent photodissociation are absorbed by H_2 in the outer layers of the cloud, effectively shielding the H_2 within it. The rate of H_2 photodissociation thus depends on the abundance and state of excitation of the H_2 as you go into the cloud. Self-shielding occurs in diffuse clouds exposed to the ISRF or in dense clouds in proximity to sources of UV photons (e.g., reflection nebulae around early-type stars or HII regions and PNe). Dust can also absorb UV photons, further limiting the process, but as we will see it dominates only when the local UV radiation field is unusually intense relative to the density of the cloud.

Self-shielding makes H_2 a very robust molecule, allowing it to exist even in the UV radiation field of the diffuse ISM.

The H_2 photodissociation rate in the presence of dust opacity and H_2 self-shielding is

$$\zeta_{diss} = \zeta_0 e^{-\tau_{gr}} f_{shield}(N_{H2})$$

where ζ_0 is the dissociation rate at the cloud surface, τ_{gr} is the dust grain optical depth, and f_{shield} is the **self-shielding factor**, which Draine & Bertoldi [1996, ApJ, 468, 269] estimated as

$$f_{shield} = \begin{cases} 1 & \text{for } N_{H_2} < 10^{14} \text{cm}^{-2} \\ \left(\dfrac{N_{H_2}}{N_0}\right)^{-3/4} & \text{for } 10^{14} \le N_{H_2} < 10^{21} \text{ cm}^{-2} \end{cases}$$

Below the threshold column density of $N_0 = 10^{14}$ cm^{-2} there is no self-shielding, whereas above it self-shielding scales as the H_2 column density to the 3/4 power.

The strong dependence on column density means we expect there to be a very sharp-edged transition between atomic and molecular gas regions as we go into a molecular cloud, much in the same way that we saw an abrupt transition between ionized and neutral gas in HII regions. This can be seen as follows. In steady state, H_2 destruction is balanced by H_2 formation

$$\zeta_{diss} n_{H_2} = R_d n_H n_{H^0}$$

Assuming low dust opacity and recalling that $n_H = n_H{}^0 + 2n_{H2}$, the steady-state density of H_2 is

$$n_{H_2} = n_H \left(\frac{\zeta_0 N_0^{3/4}}{R_d n_H N_{H_2}^{3/4}} + 2 \right)^{-1}$$

Since column density (N) and total density (n) are related by dN=n ds, we can rewrite this to solve for the approximate H_2 column density:

$$N_{H_2} = \left(\frac{R_d n_H}{4\zeta_0} \right)^4 \left(\frac{N_H}{N_0} \right)^4 N_0$$

and the H_2 abundance, X_{H2}

$$X_{H_2} = \frac{dN_{H_2}}{dN_H} = 4\left(\frac{R_d n_H}{4\zeta_0} \right)^4 \left(\frac{N_H}{N_0} \right)^3$$

The result is that there is a very sharp transition between neutral atomic hydrogen (H^0) and molecular hydrogen (H_2) going into a region of steady-state photodissociation because of the effect of self-shielding. The mid-point of the transition will occur when the gas is half atomic and half molecular which occurs when $X_{H2} = 1/4$. This transition point occurs at a column density of

$$N_{diss} \approx 3.7 \times 10^{22} \left(\frac{G_0}{n_H} \right)^{4/3} \text{ cm}^{-2}$$

where G_0 is the mean intensity of the ISRF and taking $R_d = 3 \times 10^{-17}$ cm^3 s^{-1}, the upper end of the range quoted above. Dust opacity starts to become important when $A_{1100\text{Å}} \approx 1$ hence $N_H \approx 2 \times 10^{20}$ cm^{-2}. This means that the onset of H_2 self-shielding will determine the location of the H_2/H^0 transition for $(G_0/n) < 0.02$ cm^3, which is generally true of molecular clouds illuminated by the ISRF. Near OB star-forming regions or reflection nebulae in proximity to UV-bright stars, however, $(G_0/n) \sim 1$ cm^3, and dust opacity, not self-shielding, determines the location of the molecular/atomic transition which works out to be a depth where $A_V = 2$ going into the molecular cloud.

V-3 Observed Properties of Molecular Clouds

In this section we will briefly review some of the properties of giant molecular clouds as derived primarily from observations of tracer molecules like CO. This is a research area that has become increasingly active as new and better millimeter techniques; especially millimeter interferometry and sub-millimeter imaging (e.g., SCUBA) have come into use. A thorough review of the current literature would be beyond the scope of this course, but this should give you an idea of some of the more common results quoted in recent and previous papers.

Cloud Structure

Local density estimates using line ratios often give larger densities than global mean densities found by averaging the observed molecular column densities along the line of sight. The interpretation of this is that the clouds are very clumpy, with the dense cores having typical sizes of <1 pc or smaller, and densities $>10^6$ cm^{-3}. The overall cloud itself extends for 3–20 pc on average, with a mean density of 10^{3-4} cm^{-3}. Some molecular clouds (most?) have a number of discernable cores. These are often detected as sources of molecular lines with high critical densities (e.g., CS), while the general cloud is mapped using lines of lower critical density (chiefly CO).

Within the galaxies, molecular clouds are most often seen organized into complexes with sizes from 20 to 100pc, and overall H_2 masses of 10^{4-6} M_{sun}. The distinction between "clouds" and "complexes" in terms of sizes and masses is somewhat artificial. A more precise statement is that we see a wide range of structures, from single small clouds to large complexes of clouds, with many complexes arrayed along the spiral arms of the Galaxy.

Cloud Masses

One way to estimate the mass of a molecular cloud is to integrate the column density across the face of the cloud by mapping it with millimeter interferometry.

A common alternative that is used is to assume that the cloud is only supported against its own gravity by internal thermal pressure. In this case the characteristic length scale within the cloud is the **Jeans Length**:

$$R_J \approx \left(\frac{kT}{Gn\mu^2} \right)^{\frac{1}{2}}$$

Assuming that the clouds are spherical, the mass will be the Jeans Mass:

$$M_J \equiv \frac{4\pi}{3} R_J^3 \rho_C \approx 18 M_{sun} T^{1.5} n^{-0.5}$$

where T is the kinetic temperature in K, and n is the density in cm^{-3}. If the cloud is supported against gravity by random turbulent velocities with a characteristic velocity dispersion of Δv, you can define a **Virial Mass** for the cloud"
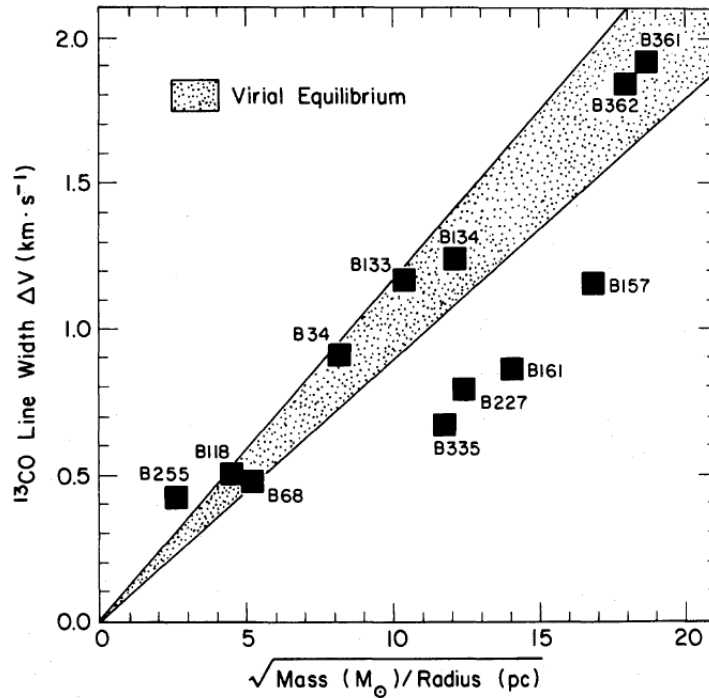
$$M_{vir} \approx \Delta v^2 \left(\frac{R}{G} \right)$$

Where R is the radius of the cloud, and Δv is the velocity dispersion of an optically thin emission line (e.g., the ^{13}CO J=1–0 line). The assumption here is that the observed velocity dispersion is just the amount needed to virialize the cloud. Computation of a virial mass requires that you can resolve the cloud (measure R). A more sophisticated analysis assumes that the cloud has a radial density profile, rather than some constant density. For a density profile that goes like 1/r, the virial mass is:

$$M_{vir} \approx 99 \Delta v_{km/s}^2 D_{pc} \ M_{sun}$$

D_{pc} is the diameter of the cloud in parsecs (see Wilson & Scoville 1990, ApJ, 363, 435 for details of how D_{pc} is defined in practice).

Comparing observations of M, R, and Δv for molecular clouds demonstrate that many clouds behave as if they are virialized, although there are clear outliers (e.g., as seen in the figure from Leung, Kutner & Mead 1982 ApJ, 262, 583 below). To be certain that optical-depth affects are not distorting the observed velocity dispersion, optically thin lines are observed so that the velocity dispersion is measured along a line of sight that passes all the way through the cloud.

^{13}CO line width versus (M/R)$^{1/2}$ [From Leung et al. 1982]

For the ^{12}CO J=1–0 line, a common analysis of the mass often applied to extragalactic CO observations is to correlate the ^{12}CO line luminosity with the virial mass. The intensity of the CO line is (I'll drop the "12" but remember it!) is the integral over the observed line profile (here in velocity units):

$$I_{CO} = \int T_A^* dv$$

I_{CO} is often quoted in units of K km s^{-1}, like we saw earlier for the H I 21-cm line. The Luminosity of the line is the integral over the cloud's face times the distance squared:

$$L_{CO} = D^2 \int I_{CO} d\Omega$$

Integrating gives:

$$L_{CO} = T_A^*(CO) \Delta v \pi R_C^2$$

where:

$$\Delta v = \text{ line width}$$

$$R_C = \text{ cloud radius}$$

$$T_A^*(CO) = \text{ peak brightness temperature of the line}$$

[Yes, the units are funny, this really is what is done in many classic CO papers, and I'll make up for this shortly.]

For spherical clouds in virial equilibrium, the velocity dispersion is:

$$\Delta v = \left(\frac{GM_C}{R_C} \right)^{1/2}$$

(equating the virial mass with the cloud mass), and the cloud's mean mass density is:
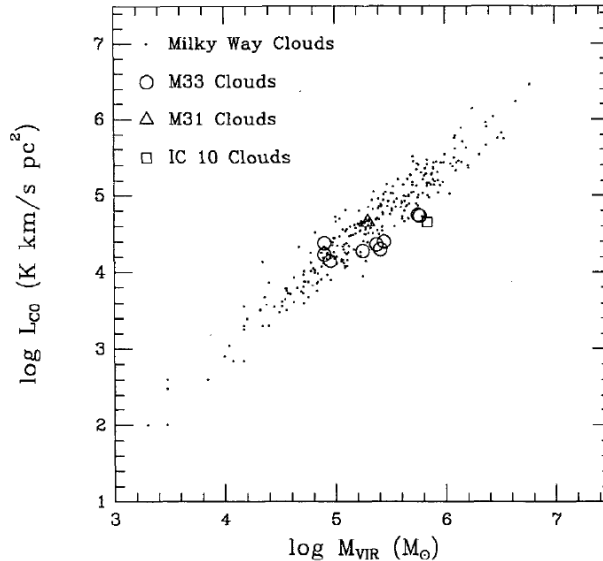
$$\rho_C = \frac{3M_C}{4\pi R_C^3}$$

Combining these gives:

$$L_{CO} = \left(\frac{3\pi G}{4\rho_C} \right)^{1/2} T_A^*(CO) M_C$$

The final step is to apply the **standard calibration** to convert the observed ^{12}CO line intensity into an H_2 column density. This calibration is based upon the good correlation observed between the ^{12}CO line intensity and the virial mass determined from ^{13}CO observations of *Galactic* molecular clouds. A typical value is:

$$\frac{N(H_2)}{I_{CO}} = 3 \times 10^{20} cm^{-2} \left(K \ km \ s^{-1} \right)^{-1}$$

The fits seem to be reasonably good for both cold molecular clouds and warmer clouds in associated with HII regions. Observations of nearby spiral galaxies for which this analysis can be performed show that the Galactic calibration appears to hold there as well (e.g., M33, Wilson & Scoville 1990, ApJ, 363,435; also Young & Scoville 1991, ARAA, 29, 581). To perform this analysis, the clouds must be resolved (so one can measure the cloud radius and derive a virial mass), thus it requires millimeter interferometry outside of our Galaxy.
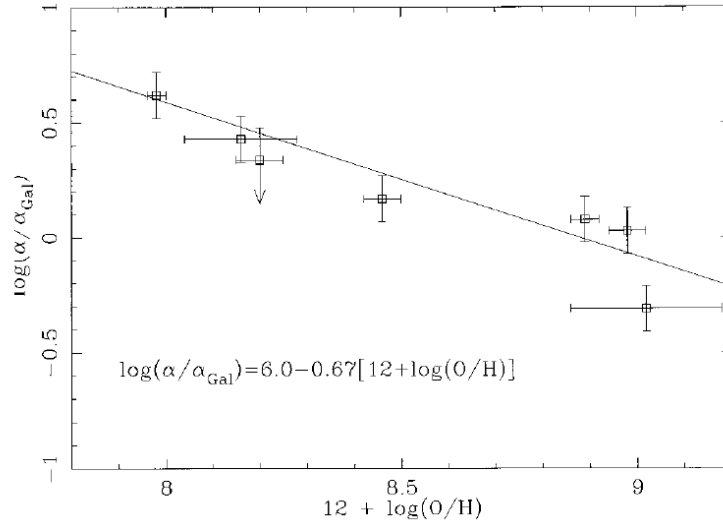

Comparison of CO luminosities and virial masses from Young & Scoville (1991)

The molecular mass derived from the CO intensity using the Galactic calibration factor above is (adapted from Wilson & Scoville 1990):

$$M_{mol} = 1.61 \times 10^{-2} d_{kpc}^2 S_{CO} \ M_{Sun}$$

Here d_{kpc} is the distance to the cloud in kiloparsecs, and S_{CO} is the integrated CO line strength in units of Janskys km s^{-1} (modern CO observations will more often express line strengths in terms of fluxes in Janskys rather than temperature units.).

The precise value of this conversion factor should depend on the density, temperature and metallicity of the gas. While the metallicity dependence has been controversial, the calibration coefficient is found to increase by a factor of ~5 for each decade of decline in O/H abundance, based on observations of molecular clouds in Local Group dwarf galaxies Christine Wilson [1995, ApJ, 448, L97] using estimates of the virial masses M_{vir} obtained using millimeter interferometry. The value of the calibration coefficient shows the expected anti-correlation correlation with the O/H abundance derived from HII regions in the same Local Group galaxies.

Average CO-to-H$_2$ conversion vs. O/H for Local Group Galaxies [Wilson 1995]

In addition, we expect that the calibration will also depend on the local conditions of the cloud being observed. One should thus be cautious in applying the calibration to any CO measurement, but unfortunately there is little empirical guidance for this, beyond the Galactic and Local Group observations described above. Sometimes it will be reasonably applicable (e.g., estimates of the H$_2$ mass of a spiral galaxy from their global CO intensity), sometimes not, but being able to judge when the latter is the case is not straightforward. Thus keep in mind that while many extragalactic CO papers will quote M(H$_2$), the real observable is L(CO), and the robustness or applicability of the Galactic calibration factor is an issue, if often an unspoken issue, in how one should interpret the results.
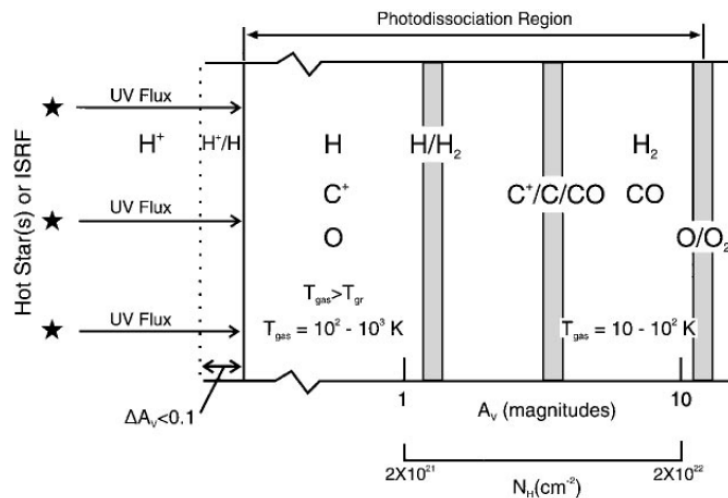
V-4 Photodissociation Regions (PDRs)

Photodissociation Regions (PDRs) are the warm, partially ionized surfaces of molecular clouds. The UV radiation field impinging upon the cloud may be either a discrete UV source, like O or B stars, or the diffuse interstellar radiation field (ISRF). The principal ionic state in a PDR is C^+, hence you will sometimes read earlier papers about "C^+ Regions" or even "CII Regions". They get their name from the fact that this is the region in which H_2 is dissociated by UV photons into HI. In a sense, we have already met PDRs in another guise, since [CII] far-IR line emission is the dominant coolant in HI regions. Since dust and molecular gas are also closely related (much of the dust in the Galaxy is in molecular clouds), PDRs are also where we get significant Far-IR emission from hot dust. In fact, as Hollenbach & Tielens state in the abstract of their 1997 Annual Reviews article on PDRs:

> "All neutral atomic hydrogen gas and a large fraction of the molecular gas in the Milky Way Galaxy and external galaxies lie in PDRs, and PDRs are the origin of most of the nonstellar infrared (IR) and the millimeter CO emission from a galaxy."

Thus, as most UV-visible emission lines arise in ionized hydrogen regions, most of the molecular and dust emission arises in PDRs. An excellent recent review of the physics of PDRs may be found in Hollenbach & Tielens 1997 [ARAA, 35, 179]. Some key papers on PDRs are Tielens & Hollenbach 1985 [ApJ, 291, 722) and Draine & Bertoldi 1996 [ApJ, 468, 269] on stationary PDRs. The classic paper on nonstationary PDRs (sometimes called non-equilibrium or time-dependent PDRs) is Bertoldi & Draine 1996 [ApJ, 458, 222].

Basic Overview of PDRs

Consider UV radiation, either from a nearby hot (types O through A and maybe early F) or the ISRF, impinging upon the face of a molecular cloud. If the UV source is a hot O or early-B type star, the UV spectrum is rich in HI ionizing photons, and you would expect to see an HII region separated from the H_2 cloud by a thin HI/HII interface. If the UV source is a later type star or the ISRF, there would be little or no HII present, and the outside of the cloud would be an HI/H_2 interface, for example, a PDR associated with a reflection nebula around a late-type B star. A schematic cross-section of a PDR is shown below.

Schematic of a PDR from Hollenbach & Tielens (1997)

Inside the HI/H_2 interface H_2 is photodissociated into HI by UV photons. The thickness of this HI/H_2 transition zone is very sharply defined because of self-shielding in H_2 (the fact that at column densities $>10^{16}$ cm^{-2} the H_2 gas becomes optically thick to in the Lyman- and Werner-band lines). Dust absorption also limits the penetration of UV photons, and dominates above $A_V \approx 2$. CO is similarly dissociated at the surface of the PDR, with the C$^+$/C/CO interface deeper in ($A_V \approx 4$). Self-shielding of CO plays an analogous role in making the transition zone very thin.

Below this region, the physics of the cloud becomes dominated by chemistry as molecules form from the dissociated gas, both on the surfaces of dust grains or in the gas-phase. This chemistry occurs in networks, dominated by carbonaceous and oxygenated compounds (see the figure of reaction networks).

The temperature in the cloud will fall slowly from a peak located near the HII/HI interface where heating is dominated by photoelectric heating by high-energy ionizing photons, into the PDR. Inside the HI/HII interface, ionization is dominated by C$^+$ (and some Si$^+$), and most molecules are dissociated.

PDR models fall into two basic classes:

Stationary PDR Models:

> These are models of steady-state configurations in which the timescale for H_2 formation on grains is short compared to either the dynamical time of the system, or the timescale for significant changes in the UV radiation field. Such models are very well developed, with a rich literature (see references in the Hollenbach & Tielens review article).

Time-Dependent and nonstationary PDR Models:

> These are models in which either the radiation field or the density is changing on timescale fast compared to the H_2 formation timescale. An example of a time-dependent configuration would a PDR associated with a star formation region in which O and B stars have recently begun to shine inside their parent molecular cloud. In these, one envisions a PDR advances ahead of an ionization front as the HII region grows within (or at the edge of) the molecular cloud.

> Nonstationary PDRs result when this ionization front catches up with the PDR and tries to pass it, and there is rapid advection of molecular material from the deep "shielded" regions into the photodissociation zone. In steady-state models, there is no transfer of material between these regions.

A fair amount of theoretical work is proceeding on both types of models. Most of this discussion will focus on stationary PDRs where the basic physics is better developed.

Heating and Cooling Balance

Two main heating mechanisms are at work in PDRs:

Photoelectric Heating:

> Far-UV photons can penetrate a dust grain and eject photoelectrons with energies of a few eV. This electron then migrates its way to the surface where it must overcome the work function, W, to break free of the grain. Whatever excess energy remains is converted into kinetic energy. As the grain becomes more positively charged, the photoelectron must also be able to overcome the Coulomb barrier that will be set up, limiting its further effectiveness for contributing to PE heating. The closer to the surface the electron is created, the more likely it will migrate to the

surface, thus small grains are expected to contribute more to photoelectric heating than large grains.

Ejection of photoelectrons by ionizing PAHs appears to be more efficient, even though as much as 50% of the energy of the photon may go into internal excitation energy rather than into ionization. To be effective, however, a PAH must be able to be ionized by a Far-UV photon with an energy below 13.6eV (the I.P. of H). Once a PAH is ionized, it will not be able to contribute to further photoelectric heating if the second ionization potential is above 13.6eV (e.g., the second IP is 16.6eV for pyrene [$C_{16}H_{10}$]).

Calculations show that the smallest dust grains play the dominant role in photoelectric heating. For an MRN mixture, half of the photoelectric heating is due to grains smaller than ~15Å, with the other half coming from grains between 15 and 100Å. Large grains make negligible contributions because the Far-UV photons are absorbed deep inside the grains (up to ~100Å deep), and the resulting photoelectrons rarely make it to the surface with enough energy to overcome the work function of the surface and escape.

UV Fluorescence heating of H_2:

Far-UV fluorescent "pumping" of H_2 molecules by the absorption of photons in the Lyman and Werner bands is followed by radiative de-excitation back into the ground electronic state. About 10–15% of these de-excitations will result in dissociation of the H_2 molecule, injecting energy into the gas as hot H atoms. Of the remaining 85-90% of de-excitations that do not result in dissociation, the UV photon emitted by the de-excitation will be quickly re-absorbed by another H_2 molecule (resonant scattering), or absorbed by a dust grain. Further, the excited ground state of H_2 can emit rotational-vibrational lines as the electron cascades into the v=0 ground state. The overall result is to provide effective coupling between the incident UV radiation field and the gas.

The gas in PDRs is cooled primarily by:

1. Emission of collisionally excited Far-IR fine structure lines arising in the ground states of neutral and ionized metals. The most important Far-IR cooling lines are: [CII]λ158μm, [OI]λ63μm & λ146μm, [SiII]λ35μm and [CI]λ609μm and λ370μm.

2. Collisionally excited near-infrared rotational-vibrational lines of H_2. These will have a fluorescent spectrum if the density is low, but at higher densities collisions with HI will thermalize the levels.

3. Rotational emission lines of CO and other abundant molecules. CO will be the most important (it is the most abundant species after H_2).

4. At high densities, collisions of molecules with cool dust grains can contribute.

If the surface of the PDR is heated by O stars (e.g., a PDR associated with an HII region at the surface of the molecular cloud – like we see in the Orion Nebula, which is a classic "Blister" HII region on the surface of the Orion Molecular Cloud 1 complex), there can be additional cooling from the region where H is partially ionized, in particular from lines like [OI]λ6300Å, [SII]λλ6716,6731Å, and [FeII]λ1.25μm and λ1.64μm lines. These latter are seen to be strong in regions like the "bar" of the Orion Nebula, an exposed ionization front from the HII region eating into the Orion Molecular Cloud.

Spectra of PDRs

The spectra of PDRs are rich in a number of features:

1. Thermal Far-IR continuum from equilibrium heating of large grains, and near-IR continuum from non-equilibrium heated tiny grains.

2. Strong Far-IR emission lines of [CII] and [OI], and weaker collisionally excited fine structure lines in the Far-IR and sub-millimeter regions.

3. Infrared emission bands from PAHs and/or tiny grains.

4. Rotational-vibrational emission lines of H_2 at near-IR wavelengths. If the densities are low, these lines can show the signatures of fluorescent excitation (as discussed previously), but at high densities the line ratios may be more characteristic of thermalized level populations, and so resemble those of collisionally excited regions.

5. Rotational lines of CO and other molecular species from deep within the PDR at millimeter and sub-millimeter wavelengths. In particular, the warmest parts of PDRs can show very highly excited lines of CO (e.g., CO J=6–5 or 7–6 transitions or even higher).

The fine-structure lines like the [CII]λ158μm line play an analogous role to the collisionally excited metal ion lines in HII regions by providing important diagnostics of the density and temperature in PDRs. These lines have critical densities in the range of 10^{3-5}cm^{-3}, and excitation energies of E/k$\approx$100–300K that are typical of conditions in PDRs. Where these have been observed (primarily with the Kuiper Airborne Observatory, ISO, and Spitzer) the densities and temperatures are consistent with the predictions of PDR models, suggesting typical densities of ~10^5 cm^{-3} and temperatures of 100–200K. The challenge of making greater use of these diagnostics in many different objects is the difficulty of observing at Far-IR wavelengths that are only accessible from space or the stratosphere.